# *Velocity refinement of PIV using global optical flow*



**Citation:** Experiments in Fluids. 2019 Oct 29;60(11):174

**As Published:** https://doi.org/10.1007/s00348-019-2820-4

**Publisher:** Springer Berlin Heidelberg

**Persistent URL:** https://hdl.handle.net/1721.1/131407

**Version:** Author's final manuscript: final author's manuscript post peer review, without publisher's formatting or copy editing

# Velocity refinement of PIV using global optical flow

**Cite this article as:** Jee Hyun Seong, Min Seop Song, Daniel Nunez, Annalisa Manera and Eung Soo Kim, Velocity refinement of PIV using global optical flow, Experiments in Fluids https://doi.org/10.1007/s00348-019-2820-4

# Velocity Refinement of PIV using Global Optical Flow

Jee Hyun Seong[1,2], Min Seop Song[1], Daniel Nunez[3], Annalisa Manera[3], Eung Soo Kim*[1]

[1]Department of Nuclear Engineering, Seoul National University, 559 Gwanak-ro, Gwanak-gu, Seoul, South Korea

[2]Massachusetts Institute of Technology, Cambridge, Massachusetts, U.S.

[3]University of Michigan, Ann Arbor, Michigan, U.S.

Tel. +82 (2) 880 7209; Fax. +82 (2) 889 2688; email: kes7741@snu.ac.kr



## Abstract

In this study, we propose a method to enhance the particle image velocimetry (PIV) velocity resolution by using global optical flow along with image warping. A global optical flow formula proposed by Brox et al. (2004) is adopted to compensate the intensity changes of PIV image pairs, which depend on the set-up and synchronization of a laser and a camera. The proposed method is quantitatively evaluated and validated using synthetic particle image pairs generated for Rankine vortices and reference DNS-based velocity data. The proposed method outperforms the conventional PIV method in capturing small scale vortex and turbulent structures due to its enhanced spatial resolution. In addition, the proposed method shows good performance in large displacement fields and varying image intensity whereas optical flow is applicable to small displacement and susceptible to image intensity variation in general. Finally, the proposed method is applied to real PIV particle images of a multiple rectangular jet flow. The results show that the proposed method successfully works out high-resolution fluid mechanical structure and quantities while preserving the conventional PIV results.

## Graphical abstract

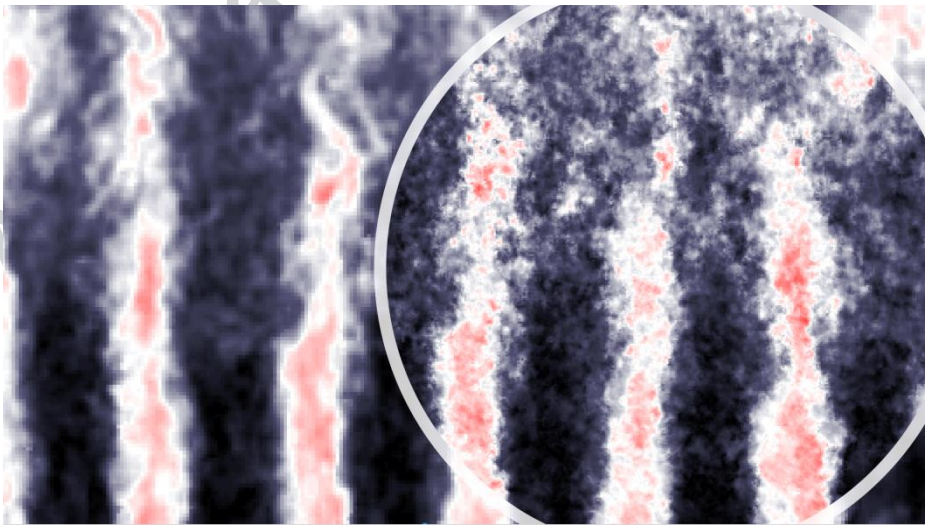

# 1. Introduction

Particle image velocimetry (PIV) is a widely-used flow visualization technique that can measure the velocity components of two- or three-dimensional fields through the successive image pairs of tracer particles in the flow field. PIV makes it possible to work out not only the qualitative form of the flow but also the quantitative hydrodynamic characteristics at the same time. Each image frame is divided into grids with the predetermined size, i.e. the interrogation area. One velocity vector that gives the maximum correlation coefficient of two successive image frames is obtained for each interrogation window. The correlation-based PIV is popularly used in various fields because of its reliability, accuracy, and robustness (Adrian 1991; Raffel et al. 2018).

However, particle image pairs should be suitably prepared for the correlation analysis. This involves various parameters such as particle size, particle number density, and particle travel distance in the images (Raffel et al. 2018; Reeder et al. 2010; Hart 2000; Willert and Gharib 1991). A proper interrogation area size is required for an accurate analysis. For example, when the interrogation window is set to be large, the measured velocity fields have a low spatial resolution. Since uniform motion within an interrogation region is assumed, estimation in regions with large velocity gradients, such as re-circulation zones, shear flow, and strong vortices, gives large errors (Jambunathan et al. 1995, Scarano 2002, Wieneke and Pfeiffer 2010, Becker et al. 2012, Thielicke and Stamhuis 2014). On the other hand, when it is set too small, the velocity vectors exceeding the interrogation area and loss-of-pairs cannot be detected, resulting in an inaccurate analysis (Scarano and Riethmuller 1999). In each window, there should be a sufficient number of particles. However, small window has a smaller number of particles, which can highly impact estimation noise (Wieneke and Pfeiffer 2010;Becker et al. 2012). Therefore, it is recommended to choose the optimum size of the interrogation area where sufficient number of particles should be available within (Huang et al. 1993) and can simultaneously provide good resolution and accuracy (Hart 2000; Scarano and Riethmuller 1999; Werely and Meinhart 2001).

For decades, efforts have been devoted to address the challenges of large velocity gradient field by increasing the resolution of correlation-based PIV. Since the fixed interrogation window size has disadvantages of smoothing out high-velocity gradients and systematically underestimates the displacements (Scarano and Riethmuller 1999, Theunissen et al. 2007), several methods have been proposed for varying window(or image) size and shape. Huang et al. (1993) deformed particle image for each single interrogation area based on the local velocity gradient priori obtained by the conventional correlation. They showed enhanced estimation on distorted particle images. However, their approach requires accurate velocity gradient calculation and higher-order interpolation scheme to compute accurate pixel relocation. Jambunathan et al. (1995) iteratively re-built the whole image based on velocity gradients. Offsets obtained in each iteration are added to the recorded displacement at each grid. However, the results of the improved technique depends on the initial estimation obtained by the conventional cross-correlation method. Scarano and Riethmuller (1999) iteratively refined the size of the interrogation areas, so called window displacement iterative multigrid (WIDIM). Followed by WIDIM, Scarano and Riethmuller (2000) proposed to iteratively deform windows. Advanced algorithms using unstructured grids, local flow adaptive window size and sampling, had been developed by Scarano (2002). Theunissen et al. (2007) proposed to adapt the number and size of the local interrogation window in unstructured grids based on the local particle density and velocity gradients. As a follow-up, Theunissen et al. (2010) suggested the ensemble-based criterion to adapt the non-isotropic windows to yield high spatial resolution in a more robust way. Apart from the square discrete interrogation window, several studies had been done with Gaussian elliptical windows. Size, shape and orientation of the Gaussian window is adapted to the local displacement direction (Di Florio et al. 2002) and velocity field curvature (Scarano 2003). Since number of particles is one of important factors to decide window size, Wieneke and Pfeiffer (2010) and Becker et al. (2012) considered quality of image signal or correlation coefficient as well as spatial fluctuations in the flow to optimize characteristics of the elliptic windows.

For above advanced correlation methods, however, the decrease in the final window size may include too few tracers to perform a reliable correlation (Theunissen et al. 2007). Therefore, the spatial resolution of the

correlation method is systematically limited by the minimum number of particles in the interrogation window (Scarano 2002). Another practical way to obtain denser velocity fields is adopting the optical flow technique, which has been originally developed for object detection in computer vision. The optical flow analyzes the variations in pixel intensities over time of successive image pairs to obtain the velocity vectors (Koenderink 1975). Compared with the correlation-based algorithm, the optical flow can obtain one velocity vector per pixel. The majority of today's progress in the optical flow technique originates from the global variational methods first proposed by Horn and Schunk (1981). Introduction of the optical flow method in flow field has started relatively recently. Ruhnau et al. (2005) adopted a global variational optical flow combined with the multi-resolution and multi-scale approach (a.k.a. coarse-to-fine or image pyramid) to cope with large displacement. Followed by, various kind of modification to the global variational optical flow formula taking into account physics of fluid flow had been vigorously proposed (Corpetti et al. 2002; Corpetti et al. 2006; Liu and Shen, 2008; Cassica et al. 2011; Cai et al. 2018). However, in standard Gaussian pyramidal approaches, successive low-pass filtering and subsampling/downsampling may lead to a loss of information (Heitz et al. 2008; Heitz et al. 2010). This can result in measurement failure for sparse and isolated particle motion, such as in 3D PIV (Alvarez 2009). To tackle the limitations in coarse-to-fine approach, attempts to use priori-known estimation done by conventional correlation to compensate large displacement have been proposed. Heitz et al. (2008) added a new functional constraining estimated displacements to be close to a sparse correlation-based vector field. In this approach, typical coarse estimation of the multiresolution scheme had been replaced with the correlation-based vectors. They added another constraint to variational optical flow that displacement estimation is consistent with the prediction by Navier-Stokes equations. Alvarez (2009) included incompressibility of the flow as a constraint when minimizing variational energy functional. They used the displacement field estimated using cross correlation to initialize the problem and to be refined. Yang and Johnson (2017) suggested refining displacement field obtained by direct correlation without sub-pixel interpolation using Liu and Shen (2008) estimator.

However, still, it seems that optical flow for PIV applications is not yet sufficiently mature compared to the robust, reliable conventional correlation-based methods in spite of its potential and advantages. The optical flow is more susceptible to experimental noise and imaging conditions (Cassisa et al. 2011). Liu et al. (2015) showed that the optical flow technique can improve the accuracy of PIV images only when the particle images are properly prepared, e.g. with relatively small particle displacement, small velocity gradients, and small illumination changes. During particle image measurement, due to varying laser output and non-uniform laser intensity distribution, obtained particle images may have different intensity profile. In order to address the image intensity-sensitivity issues in optical flow calculation and make robust estimations, we applied the intensity gradient consistent constraint adopted by Brox et al. (2004).

In this study, we propose a method of reprocessing the particle image pairs using the optical flow technique to improve the spatial resolution of the velocity vectors obtained by the conventional correlation method with multi-pass, grid refinement, and recursive window deformation. First, the particle image pairs are processed using the correlation-based PIV method and then one image is transformed based on the PIV velocity field. Then, the optical flow technique is applied to the transformed image pairs to refine the velocity vectors. We demonstrated the resolved velocity fields and evaluated the performance quantitatively using synthetic and real particle image pairs. The details of the optical flow method and PIV velocity refinement algorithm are described in the following section.

# 2. Methodology

## 2.1 Robust optical flow against intensity changes

Optical flow methods calculate the motion between two sequential images taken at time t and t+dt at every pixel position. When I(x, y, t) is the intensity of the image obtained at time t, and the position (x, y, t) is moved by dx, dy, and dt between the two images, the intensity of these two point can generally be assumed to be identical (Horn and Schunk 1981).

$$\mathrm{I}(\mathrm{x},\mathrm{y},\mathrm{z}) \approx \mathrm{I}(\mathrm{x}+\mathrm{dx},\mathrm{y}+\mathrm{dy},\mathrm{t}+\mathrm{dt}) \tag{1}$$

The right hand side of Eq. (1) can be expanded using the Taylor series.

$$\mathrm{I}(\mathrm{x}+\mathrm{dx},\mathrm{y}+\mathrm{dy},\mathrm{t}+\mathrm{dt}) = \mathrm{I}(\mathrm{x},\mathrm{y},\mathrm{t}) + \frac{\partial \mathrm{I}}{\partial \mathrm{x}}\mathrm{dx} + \frac{\partial \mathrm{I}}{\partial \mathrm{y}}\mathrm{dy} + \frac{\partial \mathrm{I}}{\partial \mathrm{t}}\mathrm{dt} \ \ldots \tag{2}$$

From Eqs. (1) and (2), the following basic optical flow equation can be obtained.

$$\mathrm{I_x u} + \mathrm{I_y v} + \mathrm{I_t} = 0 \tag{3}$$

where, $\mathrm{u} = \frac{\mathrm{dx}}{\mathrm{dt}}$, $\mathrm{v} = \frac{\mathrm{dy}}{\mathrm{dt}}$, $\mathrm{I_x} = \frac{\partial \mathrm{I}}{\partial \mathrm{x}}$, $\mathrm{I_y} = \frac{\partial \mathrm{I}}{\partial \mathrm{y}}$, and $\mathrm{I_t} = \frac{\partial \mathrm{I}}{\partial \mathrm{t}}$.

However, Eq. (3) has two unknown variables (u, v) (*aperture problem*) and, therefore, an additional equation is necessary to obtain the solution. Depending on how the constraint is provided, the methods are grouped into two categories: a local method first proposed by Lucas-Kanade (1981) and a global method pioneered by Horn-Schunk (1981). In this study, we used a global optical flow method following the recent studies on the optical flow application to PIV (Ruhnau et al. 2005; Corpetti et al. 2006; Heitz et al. 2008; Liu et al. 2015; Cassisa et al. 2011; Derian et al. 2013; Yang and Johnson 2017; Cai et al. 2018). However, the *brightness constancy assumption* may not be guaranteed for PIV depending on the set-up and synchronization of a laser and a camera. In order to compensate for this, we added the *brightness gradient constancy*, the constraint that is invariant under illumination changes (Uras et al. 1988; Brox et al. 2004). This method is known to be more reliable and robust than the original global optical flow method (Brox et al. 2004; Baker et al. 2011). The *brightness gradient constancy* assumption is expressed as follows.

$$\nabla \mathrm{I}(\mathrm{x}+\mathrm{dx},\mathrm{y}+\mathrm{dy},\mathrm{t}+\mathrm{dt}) \approx \nabla \mathrm{I}(\mathrm{x},\mathrm{y},\mathrm{t}) \tag{4}$$

By applying the second-degree Taylor expansion, the following equations can be obtained from Eq. (4)

$$I_{xx}u + I_{xy}v + I_{xt} = 0 \tag{5}$$

$$I_{xy}u + I_{yy}v + I_{yt} = 0 \tag{6}$$

In order to consider continuities in flow and prevent the outliers and gradient vanishing, we applied a further assumption about the smoothness of the flow field (Horn-Schunk 1981; Brox et al. 2004). In addition, L1 penalization, $\psi(s^2) = \sqrt{s^2 + \epsilon^2}$ ($\epsilon$: small positive constant) was adopted to achieve better stability and convergence (Brox et al. 2004; Wedel et al. 2009). $\psi(s)$ is convex with a unique minimum solution. The optical flow constraint (3), (5), (6) and the smoothness constraint were integrated into a total energy functional to be

minimized.

$$\mathrm{E}_{total} = \mathrm{E}_{data} + \alpha \mathrm{E}_{smoothness} \tag{7}$$

$$E_{data} = \int \psi \left( (I_x u + I_y v + I_t)^2 + \gamma \left( (I_{xx} u + I_{xy} v + I_{xt})^2 + (I_{xy} u + I_{yy} v + I_{yt})^2 \right) \right) dxdy \tag{8}$$

$$E_{smoothness} = \int \psi (|\nabla u|^2 + |\nabla v|^2)\, dxdy \tag{9}$$

In the above equations, α and γ are regularization parameters that assign a weight for the *smoothness assumption* and *brightness gradient constancy*, respectively. These parameters should be appropriately adjusted by the user depending on the prepared image conditions since they affect the degree of smoothness, accuracy, and robustness. For the standard variational approach, α is set from 50 to 80 and γ is 0. On the other hand, solving only data term (i.e., equation (3), (5) and (6)) by setting α=0 cannot give accurate solution. In this study, these values were determined through the iterative calibration process for various test data. In the following analysis, we used α=70 and γ=10 to provide an optimal performance. The velocity components (u, v) that minimize the total energy must satisfy the Euler-Lagrange equations of the calculus of variations. The final equations solved in this study are as follows. These Euler-Lagrange equations were assigned to each pixel independently.

$$\psi' \left( I_t^2 + \gamma \left( I_{xt}^2 + I_{yt}^2 \right) \right) \cdot \left( I_x I_t + \gamma \left( I_{xx} I_{xt} + I_{xy} I_{yt} \right) \right) - \alpha\, div(\psi'(|\nabla u|^2 + |\nabla v|^2)\nabla u) = 0 \tag{10}$$

$$\psi' \left( I_t^2 + \gamma \left( I_{xt}^2 + I_{yt}^2 \right) \right) \cdot \left( I_y I_t + \gamma \left( I_{yy} I_{yt} + I_{xy} I_{xt} \right) \right) - \alpha\, div(\psi'(|\nabla u|^2 + |\nabla v|^2)\nabla u) = 0 \tag{11}$$

The first and the second derivative terms in Eqs. (10) and (11) were calculated using the Derivative of Gaussian (DoG) and Laplacian of Gaussian (LoG) kernel, respectively. Brox et al. (2004) experimentally showed that the energy functional having second-order derivatives is still robust under noise. Since Eqs. (10) and (11) are nonlinear, a numerical scheme based on two nested fixed point iterations is applied to linearize the equations at each iteration step (Brox et al. 2004). The resulting sparse linear system is solved by a preconditioned conjugated gradient (PCG) method, which is known to be efficient and well optimized for solving a positive-definite large symmetric sparse matrix.

## 2.2 PIV velocity refinement using the optical flow

In this paper, we propose a method to improve the velocity resolution by using the optical flow while preserving the conventional PIV results. The basic algorithm is shown in Fig. 1. First, displacement and velocity fields (u, v) are obtained from two successive images (Image-1, Image-2) using conventional PIV analysis with multi-pass, grid refinement, and recursive window deformation. The displacement is used to calculate displacement information at every pixel of the target resolution via either bilinear or bicubic interpolation. Then, one of the images (Image-2 in Fig. 1) is transformed into a new image (Image-2C) by the reverse amount of the obtained velocity field (-u', -v') using either bilinear or bicubic interpolation. By this process, Image-2 becomes close to Image-1 but not perfectly matched. To reduce this deviation, the optical flow is applied pixel-by-pixel for Image-1 and Image-2C. With this analysis, the velocity deviation field (du, dv) is obtained. Finally, the PIV velocity field (u, v) and the optical flow velocity field (du, dv) are added to obtain the final velocity field. The optical flow is a method of analyzing the velocity field through the intensity change in the pixel, and thus one velocity vector can be obtained per pixel theoretically. However, it is more desirable to resize the image to match the target resolution (which can be smaller than the original image size) before an analysis in order to increase the efficiency of the analysis. In addition, unless the number density in the images is sufficient, this may cause noise in the optical flow analysis. It is another reason that resizing the images is sometimes necessary. The resizing is performed by the same interpolation method as used in the displacement field interpolation.

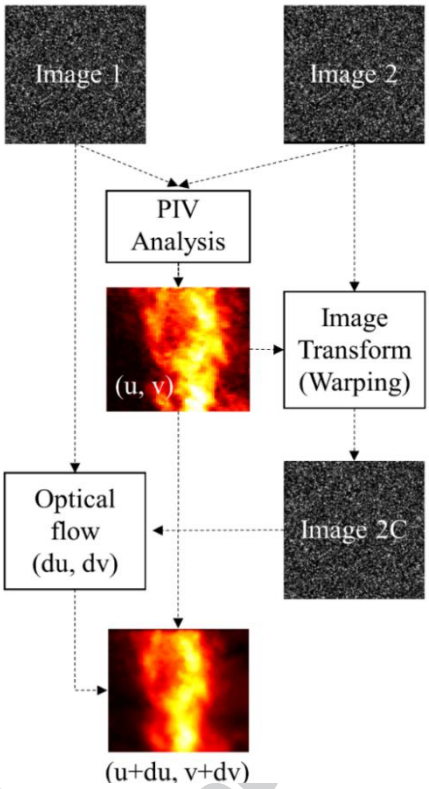


**Fig. 1** PIV Velocity Refinement Algorithm

## 3. Simulations and evaluation with synthetic image pairs

In this study, synthetic image pairs were generated by an in-house algorithm for known velocity fields of vortex and turbulent flow. The proposed method is applied to analyze these images. The reason for using synthetic particle images here is because the actual velocity field is known and therefore it is easy to evaluate the results quantitatively. PIVlab 1.43 (Thielicke and Stamhuis 2014) is used to calculate correlation matrix in the frequency domain using fast-Fourier transform (FFT) by running three passes with interrogation window size of 64×64 pixel$^2$, 32×32 pixel$^2$, and 16×16 pixel$^2$ with 50% overlap. A normalized local median filter is used to post-process the result and remove outliers. The analysis results were compared with the reference data and discussed in detail below.

### 3.1 Small vortex

A synthetic particle image of the size 300×300 pixel$^2$ is generated whereby 10,000 particles with a mean diameter of 3 pixel and size variation of 0.5 pixel are randomly distributed with out-of-plane motion of 10%. Gaussian white noise of variance 0.001 is added. A synthetic velocity field is a single Rankine vortex which has the tangential velocity of

$$u_\theta(r) = \begin{cases} \Gamma r/(2\pi R^2) & r \le R \\ \Gamma/(2\pi r) & r > R, \end{cases} \tag{12}$$

where Γ is the circulation (i.e. the maximum displacement), and $R$ is the core radius. A sample synthetic particle image pair and the analyzed velocity fields for a single vortex with the core radius of 50 pixel and

maximum displacement of 5 pixel are shown in Fig. 2. One of each eight velocity vectors in both directions obtained by the propose method is plotted in order to show a clear view of the representation. The results of the two methods show good agreement and the proposed method qualitatively well refines the velocity vectors. The analyzed velocity fields for the smaller single vortex with the core radius of 15 pixel and maximum displacement of 5 pixel are shown in Fig 3. (a) and (b). In order to make quantitative comparisons, root-mean square (RMS) errors are calculated:

RMS error for $m \times n$ domain =

$$\sqrt{\frac{1}{m\times n}\sum_{j=1}^{n}\sum_{i=1}^{m}\left[(u(i,j)-u_{reference}(i,j))^2+(v(i,j)-v_{reference}(i,j))^2\right]}. \quad (13)$$

As shown in Fig. 3 (c) and (d), the resolved data have less local RMS errors than the original one near the vortex core. The high spatial resolution allows to accurately capture the large flow variance within small area near the core. As shown in Fig. 3 (e) and (f), the analyzed velocity magnitudes are generally in good agreement with the reference values. However, the conventional PIV underestimated high velocity, where the larger RMS errors come from. It is considered that the PIV analysis averaged out the velocity near the vortex core due to its comparable interrogation window size. On the other hand, the resolved case shows good predictions on high velocity near the vortex core due to its high resolutions.

The velocity fields were used to calculate vorticity distributions. Vorticity allows analyzing the turbulent structures of the flow. Vorticity line-distributions along the centerline of the domain are shown in Fig. 4. The ground truth vorticity is uniform within the vortex and zero elsewhere showing clear vorticity transition. However, the correlation-based PIV analysis smoothed the vortex boundary due to low spatial resolution. Whereas the resolved fields visualize clearer transition border of the vorticity fields.

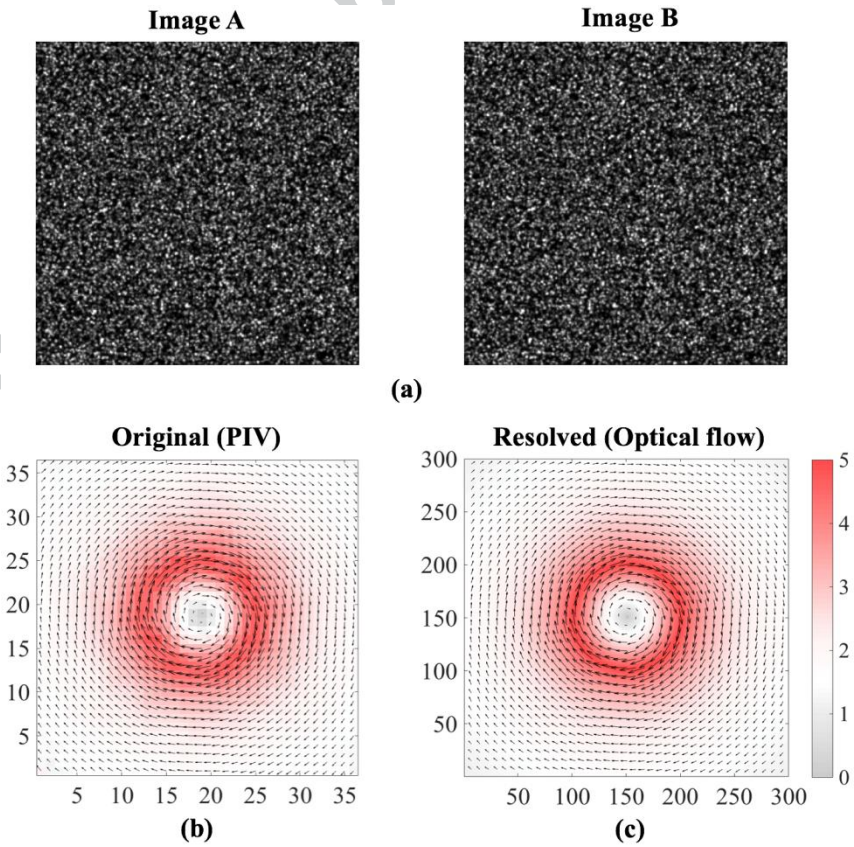


**Fig. 2** Analysis on a single vortex with the core radius of 50 pixel. **a** Synthetic particle image pair (300×300 pixel$^2$; not-to-scale); Velocity field with the magnitude map **b** obtained by the correlation method (36×36 pixel$^2$)

and **c** resolved by the proposed method (300×300 pixel$^2$;vectors are shown one-in-eight for clarity)

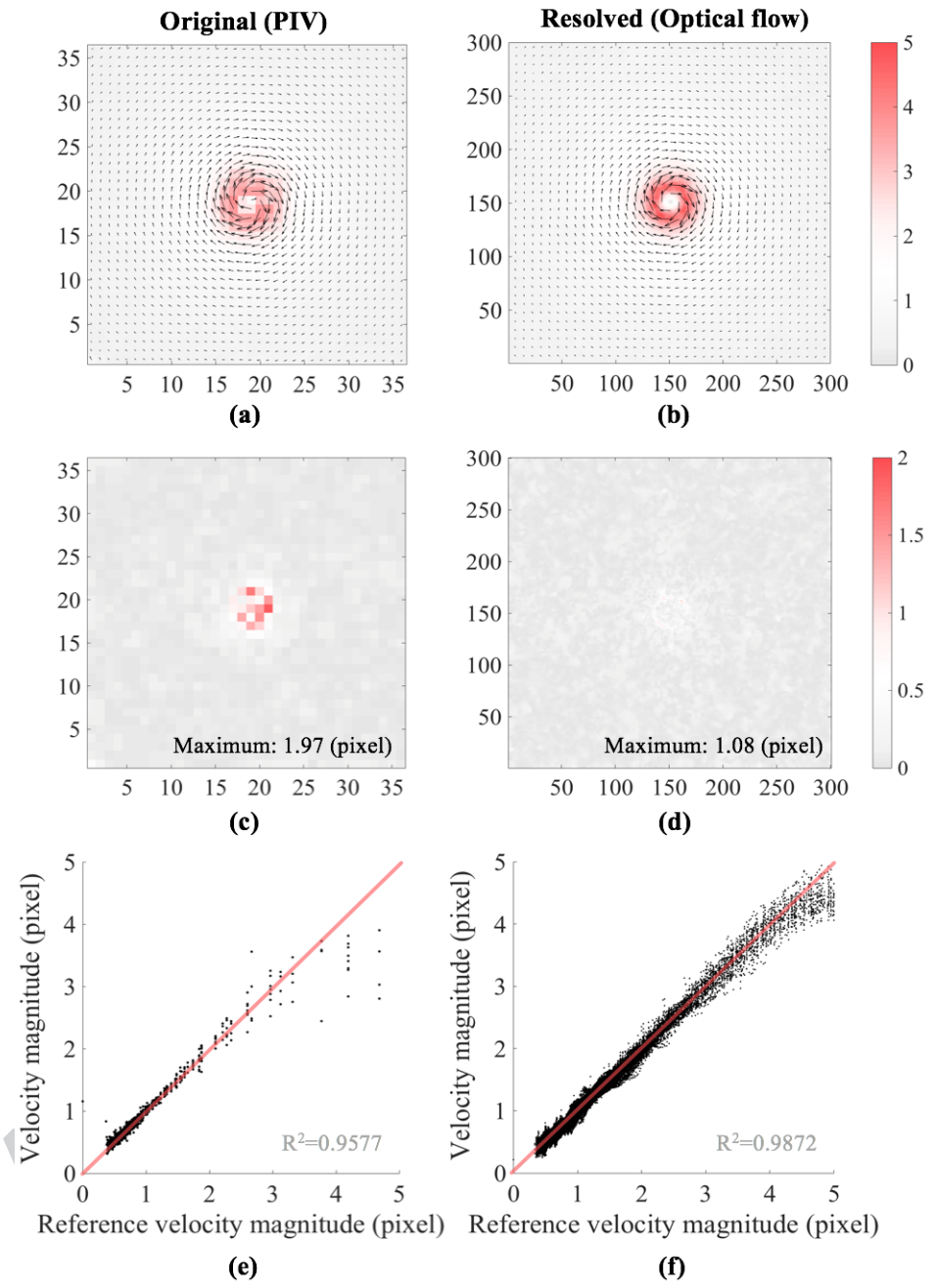


**Fig. 3** Analysis on a single vortex with the core radius of 15 pixel. Velocity field with the magnitude map **a** obtained by the correlation method (36×36 pixel$^2$) and **b** resolved by the proposed method (300×300 pixel$^2$;vectors are shown one-in-eight for clarity); Local RMS error distribution obtained by **c** the correlation method and **d** the proposed method; The velocity magnitude scatter plot for the reference and **e** the correlation method **f** the proposed method

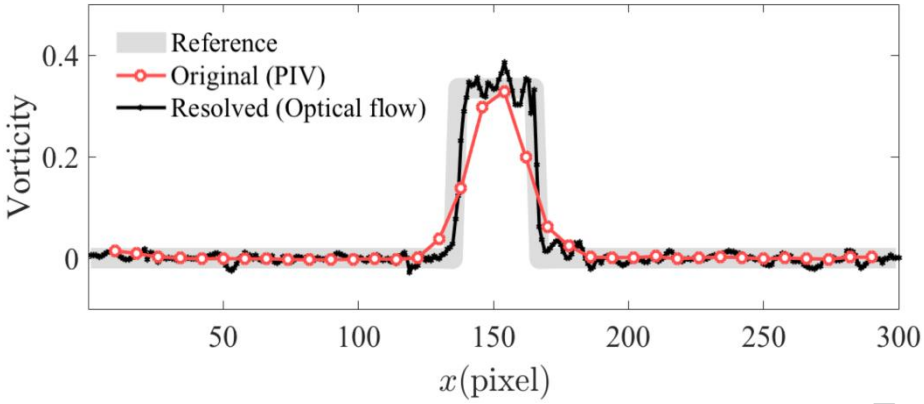


**Fig. 4** Distribution of vorticity along the centerline of the vorticity fields

## 3.2 Large displacement flow

In this section, the proposed method was applied to double Rankine vortex with different maximum displacement. Synthetic particle image pairs are generated with the size of 500×500 pixel$^2$ whereby 10,000 particles with a mean diameter of 4 pixel and size variation of 0.5 pixel are randomly distributed. Gaussian filter with the 2-pixel standard deviation was applied. No out-of-plane motion and noise are considered (Fig. 5 (a)). Synthetic velocity fields are generated by superposing double Rankine vortex with a radius of 50 pixel and center-to-center distance of 500/3 pixel on a uniform x-direction flow of 1 pixel/frame. An example of the analyzed velocity fields with maximum displacement of 7.5 pixel are shown in Fig. 5 (b) and (c). We compared the RMS error for the conventional PIV, the proposed methods, and the global optical flow adjusting Lagrange multipliers in the Horn-Schunck estimator (e.g., 200) and the Liu-Shen estimator (e.g., 2000) (Liu and Shen 2008; Liu 2017) by increasing the maximum displacement from 1 pixel to 15 pixel (Fig. 6). The global optical flow based method (Liu 2017) outperforms the correlation method at small displacement (< 6 pixel) whereas the performance degrades at large displacement fields, which corresponds with the results in Liu et al. (2015). Typically, optical flow method is more susceptible to random fluctuation than the correlation method. Meanwhile, the proposed method is robust at large displacement fields by leveraging the correlation based output.

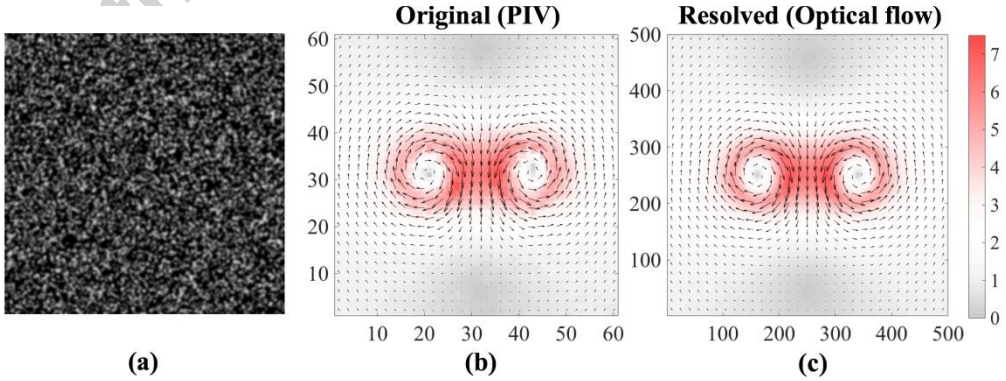


**Fig. 5** Analysis on double vortex. **a** Synthetic particle image (500×500 pixel$^2$; not-to-scale); Velocity field with the magnitude map **b** obtained by the correlation method (61×61 pixel$^2$; vectors are shown one-in-two for clarity) and **c** resolved by the proposed method (500×500 pixel$^2$; vectors are shown one-in-sixteen for clarity)

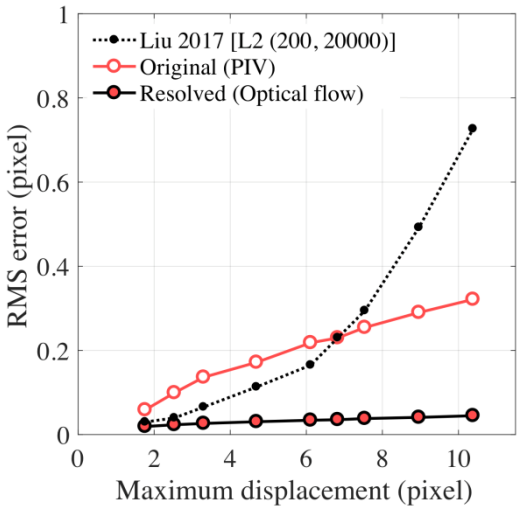


**Fig. 6** The RMS errors as a function of the maximum displacement for double Rankine vortex in uniform flow

## 3.3 Image intensity variation

During particle image acquisition, due to varying laser output, non-uniform laser intensity distribution, and non-perfect synchronization, obtained particle images may have different intensity profile. In order to address this issue, we presents here the strategy of using the brightness gradient constancy constraint, which is invariant under brightness changes. We gradually increased the overall brightness of the second particle image, as shown in Fig. 7. Each image is paired with the first image. The images with the original intensity are the same used in Session 3.2, which were generated in double Rankine vortex fields with maximum displacement of 4.7 pixel. The performance of the conventional PIV, the modified global optical flow (Liu 2017), and the proposed method ($\gamma$=0, $\gamma$=10) are compared in Fig. 8. Our optical flow algorithm when the parameter $\gamma$=0 is equivalent to the standard Horn-Schunk (Horn and Schunk 1981). The modified global optical flow (Liu 2017) performs better than Horn-Schunk. For our approach, the impact of the brightness gradient constancy constraint is quite clear. With the constraint ($\gamma$>0), the proposed method is more robust under image intensity variation than the other two methods. Brox et al. (2004) had tested their optical flow algorithm in natural scene for varying $\gamma$ value (50, 100, 200), and showed that results are fairly insensitive to parameter variations. However, users are still encouraged to adjust the parameter value to obtain the optimum performance for the different test cases. The conventional correlation would give the most accurate results when the overall intensity difference of the successive images is larger than 100%.

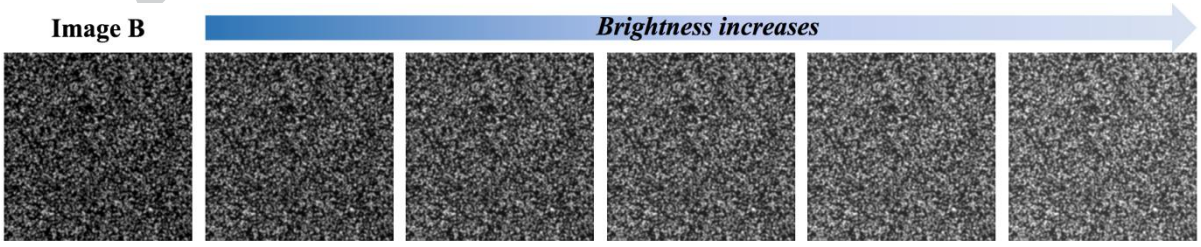


**Fig. 7** Image intensity variation. The leftmost image has the original brightness.

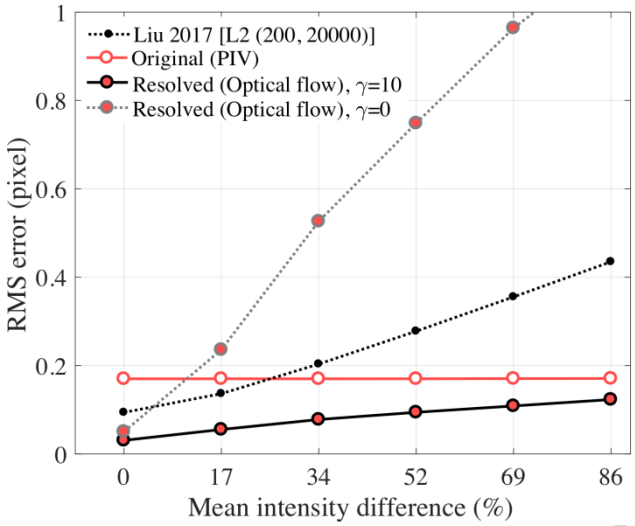


**Fig. 8** The RMS errors as a function of the image mean intensity difference (%)

### 3.4 Turbulent flow

The proposed method was applied to a synthetic particle image sequence generated from the direct numerical simulation (DNS) velocity dataset of turbulent flow with Reynolds number (Re) of 3000, Schmidt number (Sc) of 0.7, Péclet number (Pe) of 2100, and the time step of 0.01 (Carlier 2005). The main purpose of this DNS database is to obtain the exact solution of turbulent flow having a large range in the energy spectrum. The synthetic particle image and the exact velocity field of the first frame (256×256 pixel$^2$) are shown in Fig. 9 (a) and (b). As shown in Fig. 9 (c) and (d), the proposed method well resolved the PIV velocity field and the analysis results show clear turbulent features. Fig. 10 shows the comparison of the energy spectrums obtained by the reference DNS velocity field, correlation method, and the proposed method. Both the conventional correlation and the proposed method follow the correct trend at the low frequency domain, but the resolved data set has the finer cutoff ($k$=0.035) than the original data set ($k$=0.06) due to its higher resolution. This result indicates that the proposed method improves the accuracy at the smaller scales. The RMS error and the average angle error (AAE):

$$\text{AAE for } m \times n \text{ domain} = \frac{1}{m \times n} \sum_{j=1}^{n} \sum_{i=1}^{m} arccos\left( \frac{u(i,j) \cdot u_{reference}(i,j) + v(i,j) \cdot v_{reference}(i,j)}{\sqrt{u(i,j)^2 + v(i,j)^2} \cdot \sqrt{u_{reference}(i,j)^2 + v_{reference}(i,j)^2}} \right) \quad (13)$$

for the first 100 times step are provided in Fig. 11 (a) and (b). The proposed method outperforms the recently proposed optical flow approaches (Chen et al. 2015; Cai et al. 2018). Furthermore, the proposed formulation is comparable to Derian et al. (2012) and Kadri et al. (2013), where higher-order regularizers are used. The use of the non-linearized data term in the proposed energy-functional facilitates reaching the global minimum.

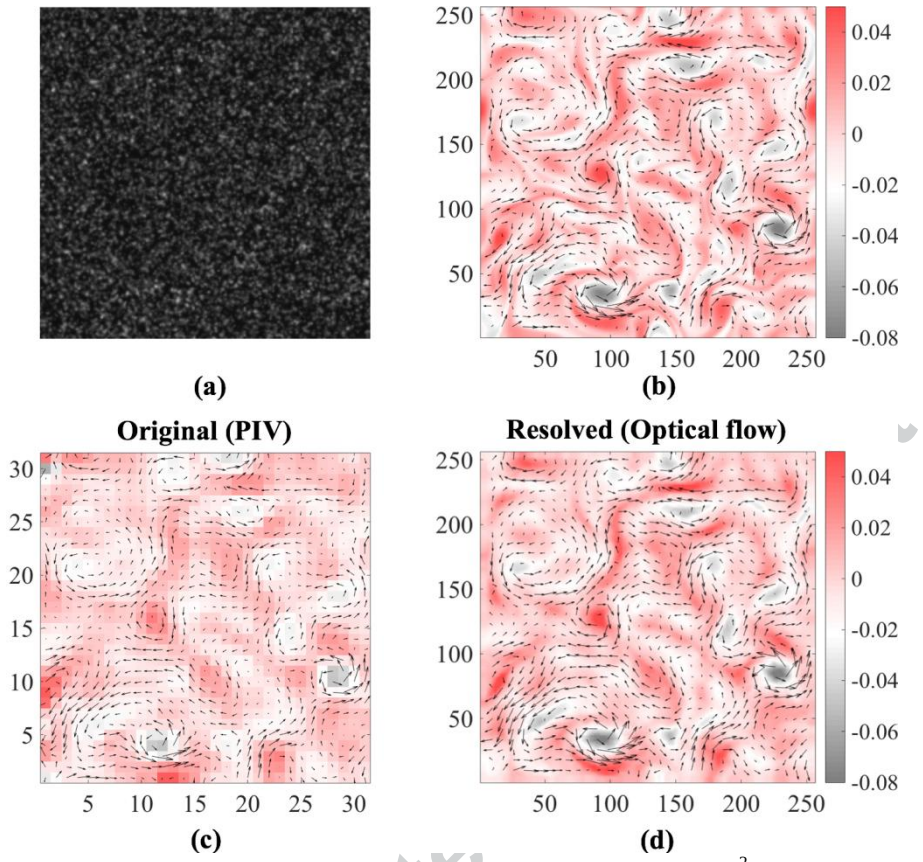


**Fig. 9** Analysis on DNS turbulent flow. **a** Synthetic particle image (256×256 pixel$^2$; not-to-scale); **b** Exact DNS velocity field with the vorticity map at the first frame; Analyzed results by **c** the correlation method (31×31 pixel$^2$) and **d** the proposed method (256×256 pixel$^2$; vectors are shown one-in-eight for clarity)

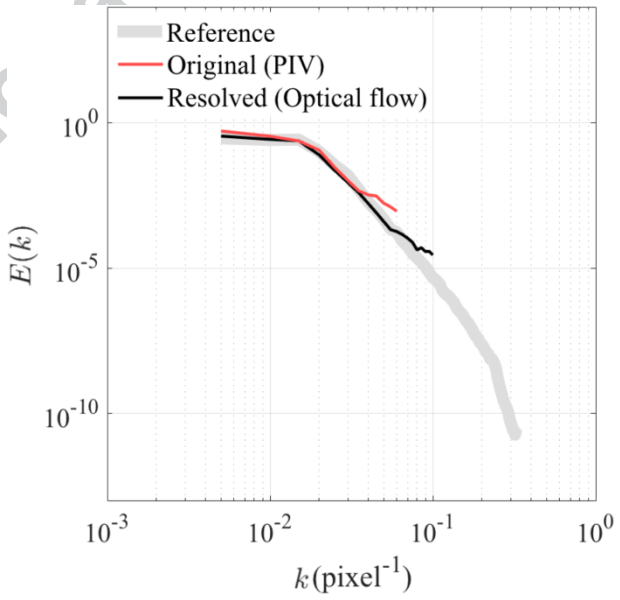


**Fig. 10** Energy spectrum of a two-dimensional turbulent flow

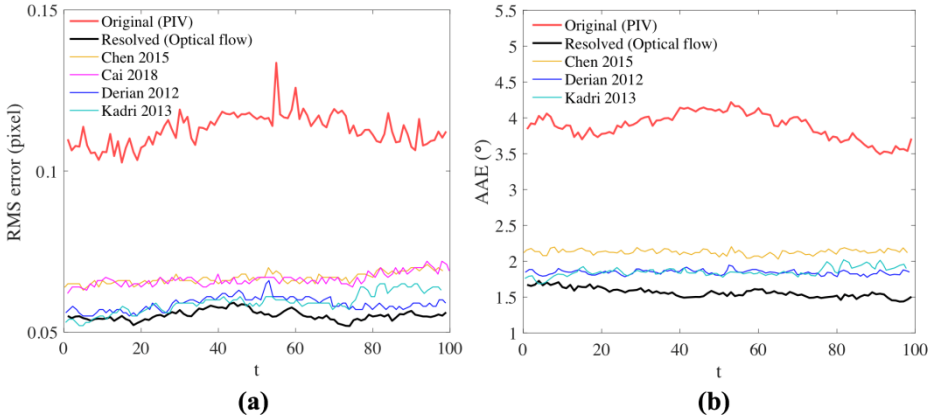


**Fig. 11** Statistical error analysis on DNS particle image sequence. **a** RMS error; **b** AEE

## 4. Experiments on real PIV image pairs

In this section, the proposed method was applied and tested on experimental data obtained by means of PIV. Experiments were conducted on the multiple rectangular jet flow in the Reactor Cavity Cooling Systems (RCCS) separate-effects test facility, built in the Experimental and Computational Multiphase Flow (ECMF) laboratory at the University of Michigan. PIV particle image pairs were obtained in six parallel rectangular jets, with jet Reynolds number of $1.38\times10^4$. For these measurements, a 532 nm Nd:YAG laser and a 12MP CMOS camera with a sensor size of 4096×3072 pixel$^2$ and pixel size of 5.5×5.5 μm$^2$ were used. The time interval between image pairs and the recording frequency for this measurement were 750 μs and 10 Hz, respectively. Lavision's DaVis 8.4 is used for the PIV analysis using three passes with an initial interrogation window size of 64×64 pixel$^2$ with 50% overlap for the first two passes, and the final interrogation window size of 32×32 pixel$^2$ with 75% overlap. The target resolution of the refined field is set to be double of PIV for the efficiency of the analysis. Fig. 12 (a) and (b) show the instantaneous velocity magnitude fields obtained by the PIV and the proposed method, respectively. The x-axis and the y-axis were scaled by the width of the rectangular jets, $L_1$=12.7mm. In addition, small sections of the velocity vector fields, constituting of the velocities in the x and y directions, are provided in Fig. 12 (c) and (d). As shown in Fig. 13, the streamwise velocity fields obtained by the two methods show very good agreement in general, and the original velocity vectors are well resolved by the proposed method by increasing the spatial resolution. Furthermore, the turbulent energy spectrum are calculated. As shown in Fig. 14, the spectrum obtained by the correlation method collapses earlier at the small scales. On the other hand, the spectrum obtained by the proposed method retains the inertial scales before reaching the energy dissipating range.

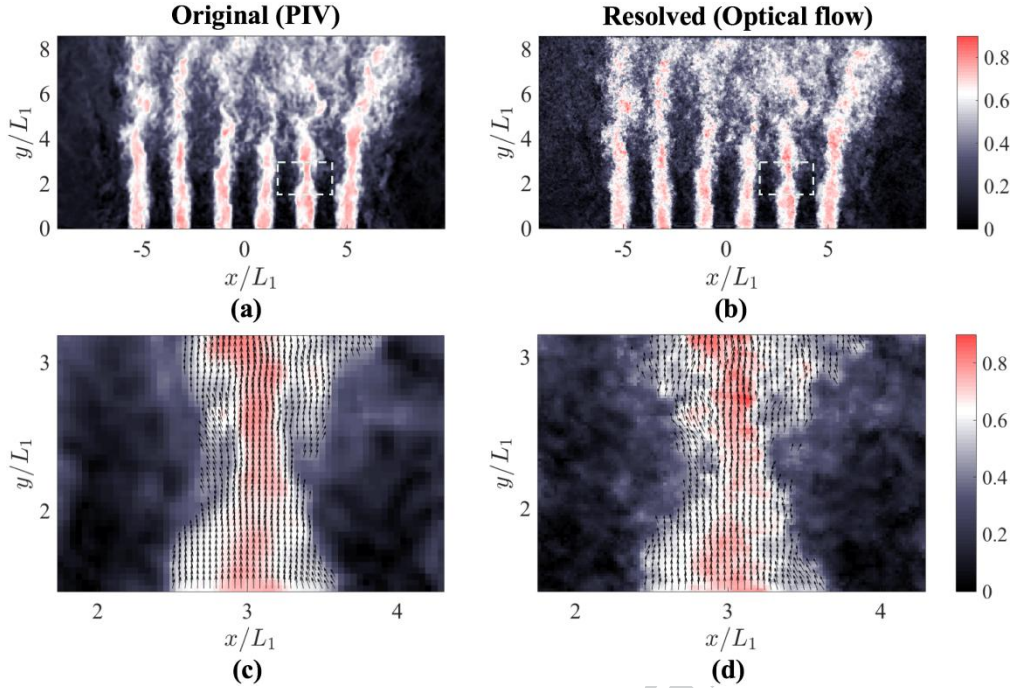


**Fig. 12** Analysis on multiple rectangular jets in the RCCS facility. Instantaneous velocity magnitude field **a** obtained by the correlation method (435×215 pixel$^2$) and **b** resolved by the proposed method (870×430 pixel$^2$; vectors are shown one-in-two for clarity). Zoomed-in velocity field by **c** correlation method and **d** proposed method

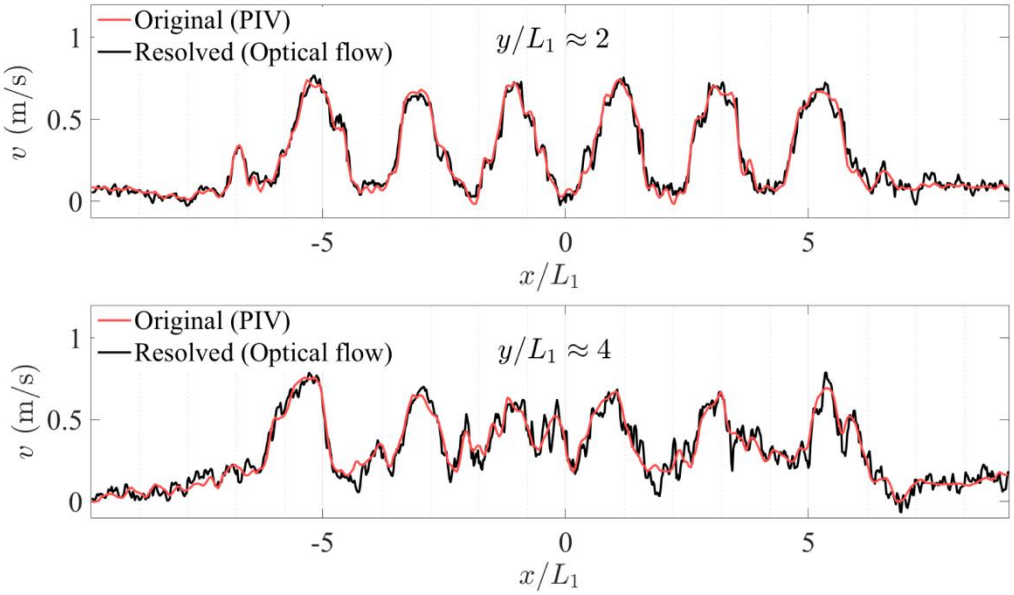


**Fig. 13** Instantaneous streamwise velocity profiles at two different $y/L_1$ axial locations

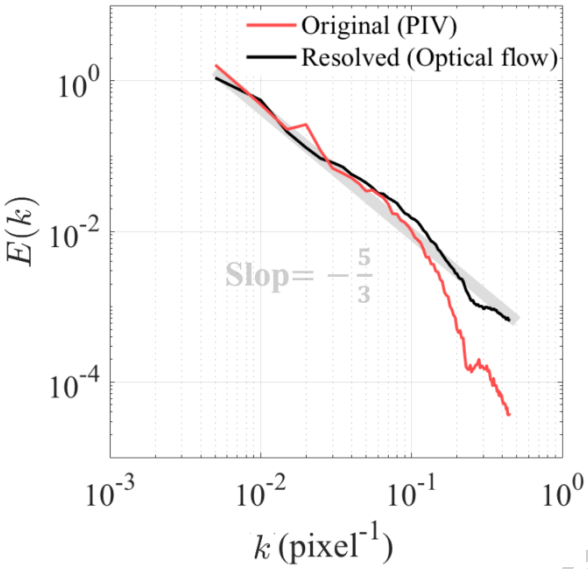


**Fig. 14** Turbulent energy spectrum of instantaneous six rectangular jet flow

## 5. Conclusions

In this paper, we introduce a method to resolve PIV velocity fields by implementing optical flow. The brightness gradient constancy assumption (Brox et al. 2004) is employed to ensure robust estimation under brightness variation depending on the PIV set-up and synchronization of a laser and a camera. The proposed method was simulated and evaluated on synthetic image pairs in vortices and turbulent flow. The PIV velocity fields are obtained with the conventional correlation with multi-pass, grid refinement, and recursive window deformation. The proposed method successfully refines PIV velocity fields and generally is in good agreement with the original data. However, the correlation method averages out the velocity due to its comparable interrogation window size, and consequently underestimates small scale flow quantities. A sensitivity study for various maximum displacements verified that the proposed method outperforms global optical flow based approach in large displacement fields since the proposed method takes advantage of the output of the correlation method. The impact of the brightness gradient constancy constraint had been clearly shown in the image brightness sensitivity study. The proposed method outperforms global optical flow based approaches in large image intensity variation. In turbulent flow, the proposed method preserves flow mechanical structures as well as turbulent quantities up to the small scale due to its enhanced resolution. In addition, the proposed method shows comparable accuracy with other optical flow approaches where higher-order regularizers are used. This is mainly due to the optical flow formula in the proposed method uses the non-linearized data term in the energy-functional which facilitates reaching the global minimum. Application of the proposed method on real PIV experimental image pairs in a multiple rectangular jet flow shows that the proposed method successfully resolved the original PIV velocity field. Obtaining high resolution data is valuable for working out quantitative flow mechanistic characteristics and understanding fluid structures. In future work, the proposed method can be used together with the other advanced correlation methods, such as flow-adaptive local window refinement scheme or Gaussian elliptic window in unstructured grids. The outcome can be leveraged to generate high fidelity experimental data for design of fluid components and validation of computational fluid dynamics (CFD) codes.

## 6. Acknowledgements

This research was supported by the National Nuclear R&D Program through the National Research Foundation

of Korea (NRF) funded by MSIP; Ministry of Science ICT & Future Planning (No. NRF-2015M1A7A01002428, NRF-2013M2B2B1075735)

## 7. References

Adrian R J (1991) Particle-imaging techniques for experimental fluid mechanics. Annu Rev Fluid Mech 23(1):261–304

Alvarez L, Castano C A, Garcia M, Krissian K, Mazorra L, Salgado A, Sanchez J (2009) A new energy-based method for 3D motion estimation of incompressible PIV flows. Comput Vis Image Und 113:802-810

Baker S, Scharstein D, Lewis J P, Roth S, Black M J, Szeliski R (2011) A Database and evaluation methodology for optical flow. Int J Comput Vis 92:1–31

Becker F, Wieneke B, Petra S, Schroder A, Schnorr C (2012) Variational adaptive correlation method for flow estimation. IEEE Transactions on Image Processing, 21(6)

Brox T, Bruhn A, Papenberg N, Weickert J (2004) High accuracy optical flow estimation based on a theory for warping. In: Proceedings of the 8th European Conference on Computer Vision 4:25–36

Cai S, Mémin É, Dérian P, Xu C (2018) Motion estimation under location uncertainty for turbulent fluid flows. Exp Fluids 59(1):8

Cariler J (2005) Second set of fluid mechanics image sequences, European Project Fluid Image Analysis and Description (FLUID). http://www.fluid.irisa.fr

Cassisa C, Simoens S, Prinet V, Shao L (2011) Subgrid scale formulation of optical flow for the study of turbulent flow. Exp Fluids 51(6):1739–1754

Chen X, Zille P, Shao L, Corpetti T (2015) Optical flow for incompressible turbulence motion estimation. Exp Fluids 56:8

Corpetti T, Mémin E, Perez P (2002) Dense estimation of fluid flow. IEEE Transactions on pattern analysis and machine intelligence 24(3)

Corpetti T, Heitz D, Arroyo G, Memin E, Santa-Cruz A (2006) Fluid experimental flow estimation based on an optical-flow scheme, Exp Fluids 40(1):80–97

Dérian P, Héas P, Herzet C, Mémin É (2012) Wavelet-based fluid motion estimation. In: scale space and variational methods in computer vision. Springer, Berlin, 737–748

Dérian P, Héas P, Herzet C, Mémin É (2013) Wavelets and optical flow motion estimation. Numer Math Theory Methods Appl 6(1):116–137

Di Florio D, Di Felice F, Romano G P (2002) Windowing, re-shaping and re-orientation interrogation windows in particle image velocimetry for the investigation of shear flows. Meas Sci Technol 13:953

Hart D P (2000) PIV error correction. Exp Fluids 29(1):13–22

Heitz D, Héas P, Mémin E, Carlier J (2008) Dynamic consistent correlation-variational approach for robust optical flow estimation. Exp Fluids 45(4):595–608

Heitz D, Mémin E, Schnorr C (2010) Variational fluid flow measurements from image sequences: synopsis and perspectives. Exp Fluids 48:369-393

Horn B K, Schunck B G (1981) Determining optical flow. Artif intell 17(1-3):185–203

Huang H T, Fiedler H E, Wang J J (1993) Limitation and improvement of PIV. Part2: Particle image distortion, ad novel technique. Exp Fluids 15:263-273

Jambunathan K, Ju X Y, Dobbins B N, Ashforth-Frost S (1995) An improved cross correlation technique for particle image velocimetry. Meas Sci Technol 6:507-514

Kadri-Harouna S, Dérian P, Héas P, Memin E (2013) Divergence-free wavelets and high order regularization. Int J Comput Vis 103(1):80–99

Koenderink J J (1975) Invariant properties of the motion parallax field due to the movement of rigid bodies relative to an observer. Opt Acta 22(9):773–791

Liu T, Shen L (2008) Fluid flow and optical flow. J Fluid Mech 614:253–291

Liu T, Merat A, Makhmalbaf M H M, Fajardo C, Merati P (2015) Comparison between optical flow and cross-correlation methods for extraction of velocity fields from particle images. Exp Fluids 56:166

Liu T (2017) OpenOpticalFlow: An open source program for extraction of velocity fields from flow

visualization images, Journal of Open Research Software 5(1)
Lucas B, Kanade T (1981) An iterative image registration technique with an application to stereo vision. In Proceedings International Joint Conference on Artificial Intelligence, Morgan Kaufmann Publishers, San Francisco, CA, 674–679
Raffel M, Willert C E, Scarano F, Kahler C J, Wereley S T, Kompenhans J (2018) Particle image velocimetry: a practical guide, Springer, 3rd ed
Reeder M F, Crafton J W, Estevadeordal J, DeLapp J, McNiel C, Peltier D, Reynolds T (2010) Clean seeding for flow visualization and velocimetry measurements. Exp Fluids 48(5):889–900
Ruhnau P, Kohlberger T, Schnörr C, Nobach H (2005) Variational optical flow estimation for particle image velocimetry. Exp Fluids. Vol. 38(1):21–32
Scarano F, Riethnuller M L (1999) Iterative multigrid approach in PIV image processing with discrete window offset. Exp Fluids 26(6):513–523
Scarano F (2002) Iterative image deformation methods in PIV. Measurement Science and Technology 13(1):R1
Scarano F (2003) Theory of non-isotropic spatial resolution in PIV. Exp Fluids 35:268–277
Theunissen R, Scarano F, Riethmuller M L (2007) An adaptive sampling and windowing interrogation method in PIV. Meas Sci Technol 18:275-287
Theunissen R, Scarano F, Riethmuller M L (2010) Spatially adaptive PIV interrogation based on data ensemble. Exp Fluids 48:875-887
Thielicke W, Stamhuis E J (2014) PIVlab – Towards User-friendly, Affordable and Accurate Digital Particle Image Velocimetry in MATLAB, Journal of Open Research Software 2(1)
Uras S, Girosi F, Verri A, Torre V (1988) A computational approach to motion perception. Biol Cybern 60:79–87
Wedel A, Pock T, Zach C, Cremers D, Bischof H (2009) An improved algorithm for TV-L1 optical flow. Statistical and geometrical approaches to visual motion analysis. Springer, Berlin, Heidelberg, pp23–45
Wereley S T, Meinhart C D (2001) Second-order accurate particle image velocimetry. Exp Fluids 31(3):258-268
Wieneke B, Pfeiffer K (2010) Adaptive PIV with variable interrogation window size and shape. 15th Int. Symp. On Applications of Laser Techniques to Fluid Mechanics, Lisbon, Portugal, 05-08 July
Willert C E, Gharib M (1991) Digital particle image velocimetry. Exp Fluids 10(4):181–193
Yang Z, Johnson M (2017) Hybrid particle image velocimetry with the combination of cross-correlation and optical flow method. J Vis 20(3):625–638